Chapter 5

The Sinuous Antenna

KISS: Keep It Simple, Stupid!

– *Ancient Engineering Proverb*

5.1 Introduction

Arrays with broadband pixels will increase the optical throughput of a camera. In this chapter we describe a novel modification of the sinuous antenna, which has five valuable properties. The antenna:

1. is **broadband** over *at least* 1.5 octaves
2. is **planar** and thus scalable to large arrays
3. is **dual-polarized**, with low cross-polarization
4. has **high gain**, to match telescope optics
5. has a **stable impedance** with frequency.

We start this chapter with a discussion of log-periodic antennas, but identify polarization wobble as a common flaw. The sinuous antenna is a special type of planar log-periodic that has an acceptable level of wobble. In free space, the sinuous antenna is self-complimentary and we discuss how this influences the input impedance of our lens-coupled antenna. Finally,

we show measurements of 1-12GHz scale-models to demonstrate the antenna's promising beam characteristics. The sinuous antenna had not been previously studied on a contacting lens, so these measurements were an important step to confirm antenna properties before fabricating the millimeter-wavelength devices in the following chapters.

5.2 Log-Periodic Antennas

Maxwell's Equations lack an intrinsic scale, so if one rescales the physical dimensions of a system, the solutions will be unchanged aside from a reciprocal rescaling of the frequencies. An infinite spiral antenna with arms following $r = e^{a\theta}$ also lacks any specific dimensional scales. So rescaling this antenna will reproduce the exact same antenna up to a rotation. Since both Maxwell's equations and the antenna are scale invariant, the beam and impedance properties are the same for all frequencies (*Rumsey* [1966]). In reality, the antenna must terminate at some finite inner and outer radii which determine the upper and lower frequency band-edges. But aside from this restriction, the continuous bandwidth of these antennas can be arbitrarily large. Unfortunately, these antennas couple to circularly polarized waves and it is not possible to make them dual polarized. Since we require dual polarized antennas that receive a linear polarization, spiral antennas are not an appropriate choice for our application.

Log-periodic antennas are closely related to the frequency independent spirals, but they are invariant *only* when rescaled by a factor of σ (*Rumsey* [1966]). An example of this is shown in Figure 5.1(a), where σ =10%. Properties such as impedance and beam shape of these antennas will repeat everytime the frequency f_n is rescaled to f_{n+1} by a multiplicative factor of σ, or equivalently whenever $\log(f_n)$ is changed by an additive factor of $\log(\sigma)$:

$$f_{n+1} = \sigma f_n$$

$$\log(f_{n+1}) = \log(f_n) + \log(\sigma)$$

If σ is sufficiently small, then these properties will undergo only minor variations within each log-period. As above, the inner and outer termination scales fix the the upper and

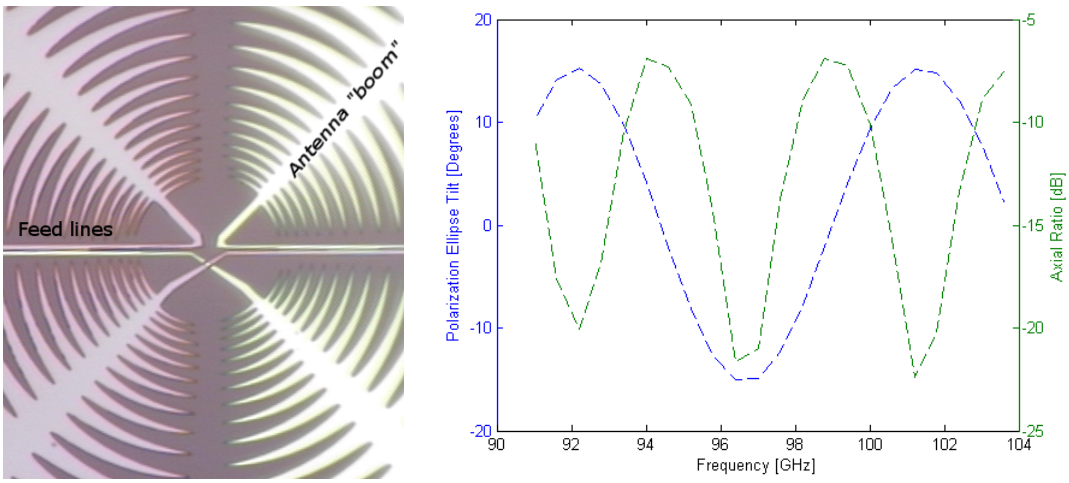

(a) Early Log-Periodic Antenna

(b) Simulated Polarization Tilt and AR

Figure 5.1. Photograph showing the interior of an early Log-Periodic Antenna. The photo is roughly 100 μm on a side, but the entire antenna has a $\sim$ 3mm diameter. The plot at right shows simulated polarization tilt (blue, left axis) and Axial Ratio (dashed green, right axis) against frequency for for the antenna without the horizontal feeds. Even without the feeds, the polarization performance is poor.

lower band edge frequencies. Fortunately, these antennas couple to linear polarizations and it is possible to fold-two antennas together to make a dual-polarized pixel.

Figure 5.1(a) was fabricated in the Fall of 2006 in an early attempt to coupled a broad-band antenna with a contacting lens to TES bolometers. It is a dual-polarized version of the original planar log-periodic antenna pioneered by DuHammel and Isbel in the 1950s (*DuHamel and Isbell* [1957] and *Engargiola et al.* [2005]) . When we rotated a polarizing grid between the detector and a chopped thermal load, the received power only dropped to $\sim$ 70% of peak (*O'Brient et al.* [2008a]); if the antenna efficiently discriminated between linear polarizations, this figure should have been no more than a few percent. ADS simulations revealed that the feed lines coupled the orthogonal sets of arms to produce an elliptically polarized beam with large axial ratio (defined in figure 5.2). But even if the feeds are moved onto the backs of the antenna booms to supress this coupling, polarization problems persist.

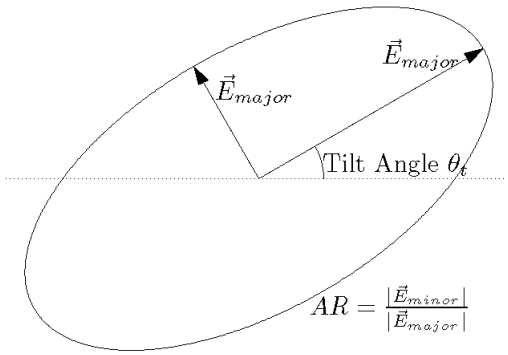

Figure 5.2. Axial ratio and Polarization tilt defined. The tilt measures the angle of the semi-major axis to a reference line while the Axial Ratio AR is the ratio of field strength on the semi-minor and semi-major axes. AR=0 for linearly polarized fields while AR=1 for circularly polarized fields.

5.3 Polarization Wobble

The polarization ellipse is the curve traced by the electric fields of a free-traveling electromagnetic wave; it's associated tilt and axial ratio are defined in Figure 5.2. A planar log-periodic antenna's polarization tilt is not fixed for all frequencies; it "wobbles" as frequency changes, repeating every log-period (*Kormanyos et al.* [1993] and *Gitin et al.* [1994]). Figure 5.1(b) shows the ADS simulated polarization tilt on boresight vs frequency for our planar log-periodic *without* the feedlines. This effect arises because the radiating fins protruding from the antenna boom alternate sides and are not parallel. Non-planar dual-polarized antennas have been built for the Allen Telescope Array that avoid this effect by bending the four arms into a pyramidal endfire antenna (*Engargiola* [2003]). However, this design is not planar and not amenable to thin film production; it would be challenging to scale them to kilopixel arrays.

Since our bolometers integrate the signal over a relatively wide band-width of 30%, it is imposible to perfectly align the antenna to a polarized test source for every frequency in the band. This rapid and large-amplitude wobble leaks as much as 13% of the crossed-polarization's power into a specific channel. Since we plan to difference two orthogonal polarization channels within a pixel, this will subtract away, but only at the expense of optical efficiency.

Figure 5.1(b) also plots the axial ratio AR. For a planar log-periodic antenna in free space, this number is very low and the beam is linearly polarized. But on a half-space of silicon, simulations suggest that the AR can climb to -8dB between tilt extrema where the beam becomes elliptically polarized. This is a second mechanism that leaks another 15% of the crossed-polarization and further degrades the efficiency. Our collaborators at UCSD have seen these effects in prior studies as well (*Kormanyos et al.* [1993]).

5.4 The Sinuous Antenna

The sinuous antenna (pictured in 5.3(a)) is a specific type of log-periodic that has an extensive heritage in the defense industry (*Bond* [2010]) ever since it's invention in the late 1980s. The edges of the switch-backing arms follow the defining equation (*DuHamel* [1987]):

$$\phi = \alpha \sin \frac{\pi \ln(r/R_o)}{\ln \tau} \pm \delta \qquad \text{for } R_o < r < R_o \tau^N \tag{5.1}$$

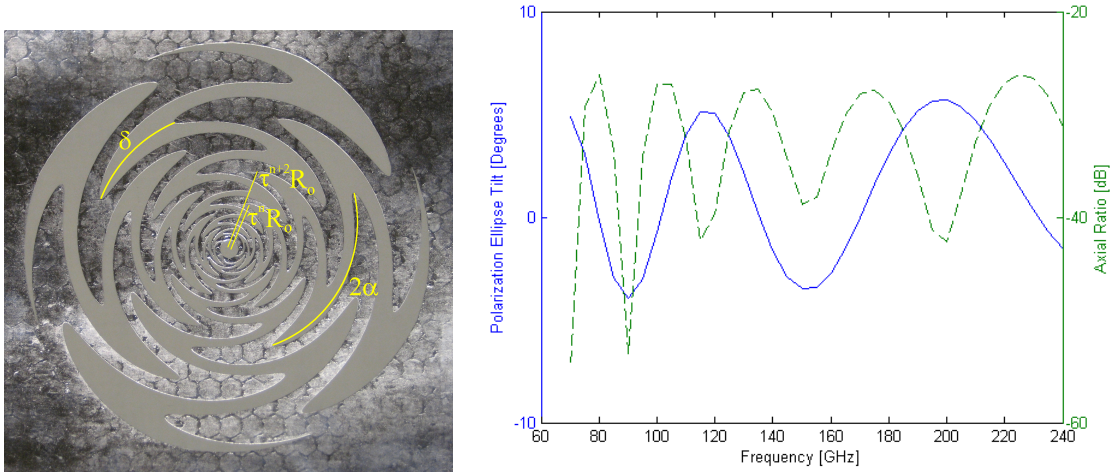

(a) A Sinuous Antenna

(b) Simulated Polarization Tilt and AR

Figure 5.3. Photograph showing a 1-3GHz scale model Sinuous; the hex pattern on the metal is an artifact of the deposition process. The plot at right shows simulated polarization tilt (blue, left axis) and Axial Ratio (dashed green, right axis) against frequency, much improved over the other log-periodic antenna.

Each of the four arms snake through an angle of $\pm\alpha$ every rescaling of τ^2. The angle δ determines the angular width of each arm and is used to control the antenna impedance

(see Section 5.6). Typical values of α are between 30^o and 70^o , while typical values of τ are between 1.2 and 1.5. This antenna is inherently dual-polarized. If we excite a pair of opposite arms with equal power and 180^o phase difference, they will couple to one of the two linear polarizations (*Saini and Bradley* [1996]).

The antenna is very similar to the log-periodic antenna of the previous section, but the boom in the center of each arm was sacrificed to merge the teeth into a continuous winding structure. ADS simulations suggest that power radiates predominantly from the sections between the switch-backs, and those sections are more closely aligned than the teeth of the classic log-periodic in Figure 5.1(a). As a result, the wobble amplitude is much lower and the axial ratio is greatly suppressed as well, as seen in Figure 5.3(b) (*O'Brient et al.* [2008b]). The antenna in this simulation has $\tau = 1.3$. Simulations also suggest that antennas with even smaller values of τ have even lower amplitudes of wobble, but they are difficult to fabricate. We only measured antennas in this thesis with $\tau = 1.3$.

The sinuous emits and radiates long wavelengths from the exterior regions and short wavelengths from the interior regions, preferentially along the $\lambda/2$ sections between the switch-backs. For an antenna driven to couple to linear polarizations, the opposite arms act as a two element array separated by $\lambda/2$, analogous to the crossed double-slot antenna. The outer-most radius $R_{out} = R_o\tau^N$ of the antenna fixes the low frequency cutoff:

$$\lambda_L/4 = R_{out}(\alpha + \delta) \tag{5.2}$$

The antenna requires a buffer region separating the feedlines from the high frequency radiating cells to maintain useful beam patterns and impedance (*DuHamel* [1987]). Most engineers conservatively pick $R_{in} = R_o$ such that

$$\lambda_H/8 = R_{in}(\alpha + \delta) \tag{5.3}$$

The useful polarization properties of the sinuous are not surprising since it is the simplest broadband generalization of the crossed-double slot antenna from Chapter-4. Topologically, the crossed double-slot is similar to a ring-slot antenna (*Raman and Rebeiz* [1996]), and our

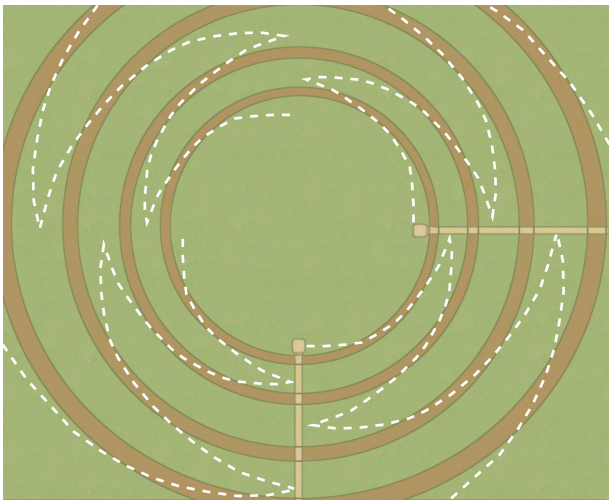

Figure 5.4. Nested Rings: The crossed double-slot antenna is similar to a single ring slot antenna. Nested rings (rust colored) with microstrips crossing into the interior do not work as a broadband antenna because the high-frequencies couple to the high-order modes of the outer rings instead of the fundamental modes of the interior. However, if we deform each quadrant of the rings into the curves shown in white dashed lines, then we open a continuous path of ground plane (green) for the microstrips to drive the antenna in the center.

collaborators at UCSD have already explored a set of two and three concentric ring-slots as a broadband alternative (*Behdad and Sarabandi* [2004]). They found that the planar transmission lines couple the high frequencies to the outer rings before they can reach the interior, leading to poor efficiency and low quality patterns at the upper band-edge (*Edwards* [2008]).

However, we can partition the rings into four quadrants and construct switch-backed curves in each to open-up a continuous stretch of ground from the exterior to interior. The result is an antenna that mimics the original rings, but is also nearly identical to the sinuous. This heritage is clear in Figure 5.4. DuHammel, the antenna's inventor, found that curves with constant width, such as those sketched in dashed white in the figure, produce unacceptable reflections at the highly inductive switchbacks and that the widened turn-arounds from Equation 5.1 capacitively load each arm to cancel out that inductance. Widening the switchbacks also interlocks the arms, which aligns the radiating $\lambda/2$ sections and suppresses wobble (*DuHamel* [1987]).

5.5 Driving a planar sinuous antenna

All log-periodic antennas must couple to their driving transmission lines at the high frequency end (*Rumsey* [1966]). If fed at the low end, the high frequency modes will never reach the regions where they should radiate; instead, they will excite high-order modes in the larger low frequency elements and form a non-Gaussian beam with low efficiency. This is identical to the problem UCSD experienced with the nested slot-rings. For planar log-periodic antennas, the high-frequency area is in the center, which is challenging to access if fed with planar transmission lines.

Historically, the sinuous was fed with coaxial cables normal to the antenna's plane (*Saini and Bradley* [1996]). However, this method is not amenable to the thin-film fabrication that we need to construct large arrays of millimeter-wavelength devices. Alternatively, some researchers have placed detectors (Diodes or Hot Electron Bolometers) in the center (*O'Brient et al.* [2008b] and *Liu et al.* [2009]). While this approach is acceptable for the scale model tests described in Section 5.7, it would preclude channelizing with microstrip circuits.

A third option is to run microstrip transmission-lines between interior and exterior down the backs of the antenna arms, using the arms as finite ground planes. This has already been used for spiral-antennas (*Nurnberger and Volakis* [1996] and *Dyson* [1959]), and we have found that it works for the sinuous as well. Examples of this feed are visible in Figure 5.6. Simulations suggest that power will negligibly leak from the microstrip to the adjacent slots provided that the line does not come within a dielectric thickness of the edge. For the devices described in the following chapters, this required clearance is 0.5 μm.

5.6 The Sinuous Antenna's Input Impedance

In free-space, a planar antenna's compliment is the same antenna but with metal and slots exchanged. Because electric fields orient themselves across the slots and tangent to the plane of the antenna, a slot will have normal magnetic fields and act as a perfect magnetic

conductor to fictitious magnetic currents. These currents are defined exactly like those on the surface of the lens in the previous chapter. If an antenna produces fields $(\mathbf{E}, \mathbf{H})$ (both near and far), it's compliment will have exchanged magnetic and electric currents that radiate dual fields:

$$\begin{aligned} \mathbf{E}' &= -\eta_o \mathbf{H} \\ \mathbf{H}' &= \mathbf{E}/\eta_o \end{aligned} \tag{5.4}$$

where η_o is the impedance of free space. Meanwhile the total currents and voltages between each feeding port are proportional to line integrals of the fields there:

$$\begin{aligned} V &= -\int \mathbf{E} \cdot \mathbf{dx} = -a\,|\mathbf{E}| \\ I &= \frac{1}{\mu_o} \oint \mathbf{H} \cdot \mathbf{dx} = \frac{2b}{\mu_o}\,|\mathbf{H}| \end{aligned} \tag{5.5}$$

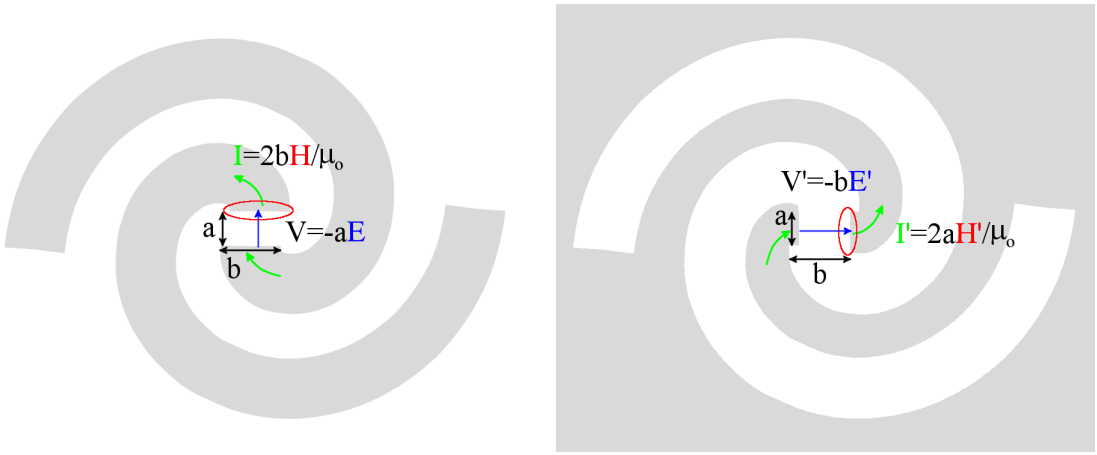

(a) A one-port antenna

(b) Antenna Compliment

Figure 5.5. Figure 5.5(a) is a two port spiral antenna, where gray is metal, white is slot. Electric and Magnetic fields are shown in blue and Red. Figure 5.5(b) is the compliment. Since the antenna is nearly self-complimentary, if it continued indefinitely, the impedances $Z = E/H$ and $Z' = E'/H'$ would be nearly equal, constant, and real

where a is the distance between the terminals and b the width of each (See Figure 5.5). Similar equations relate (V',I') to (E',H') on the complimentary antenna, but with a and b exchanged. Finally impedance matrices Z_{ij} and Z'_{ij} relate the voltages to the currents

at the ports of each antenna. Eliminating all variables but the impedances from Equations 5.4 and 5.5 relates Z'_{ij} to Z_{ij}. For the simple case of a two conductor antenna with just one port, this relationship is known as Babinet's principle (*Booker* [1946]):

$$ZZ' = (\eta_o/2)^2 \tag{5.6}$$

An antenna is *self*-complimentary when the antenna and compliment are identical. In this case, $Z{=}Z'{=}\eta_o/2{=}189\Omega$. The impedance of such antennas is real and independent of frequency (*Rumsey* [1966] and *Mushiake* [1996]). Examples of these can include two-armed bow-tie, spiral, and log-periodic antennas. The sinuous antenna is self-complimentary provided that the angular width of each arm is $\delta = 22.5^o$. However, it is a four-port structure, so we cannot calculate it's impedance without a more general form of 5.6 that relates 4×4 impedance matrices. Deshampes formula does this for the special case of N-armed rotationally N-point-symmetric antennas, and it's simplest form is in the basis where the impedance matrix is diagonalized:

$$Z_m Z'_m \sin^2\left(\frac{m\pi}{N}\right) = \left(\frac{\eta_o}{4}\right)^2 \tag{5.7}$$

where $m{=}[1, 2, ..., N]$ is one of N eignemodes, denoted M_n (*Deschamps* [1959]). In this basis, the impedance relates the voltages present on all the arms when current is applied to all the arms in one of the modes. In particular, the current applied to each arm $n = [1, 2, ..., N]$ for these modes is

$$I_{m,n} = e^{i2\pi\frac{mn}{N}} \tag{5.8}$$

where by convention, the the arms' labels n reflect their circumferential ordinality. For an antenna with $N{=}4$ arms, the M_0 and M_2 modes induce 0^o and 180^o phase shifts between each neighboring arm, driving even-symmetry modes on the antenna. The beam patterns from these cancel on boresight and are not useful to us. The other modes M_1 and $M_3{=}M_{-1}$ drive $\pm 90^o$ phase shifts between the arms. Their beams do not vanish on

boresight, launching left and right handed circularly polarized radiation. For a given mode, all arms have the same impedance relative to a virtual ground at center, and the $m = \pm 1$ modes are degenerate. When the antenna is self-complimentary ($Z_m = Z'_m$), the arms for both modes will have $Z_{\pm 1} = \eta_o/(2\sqrt{2})$ relative to ground. Figure 5.6 displays the effective circuit over photographs of our fabricated millimeter-wavelength devices, where each arm sees the same impedance $Z_{\pm 1}$. These impedances are real and independent of frequency, so free space sinuous antennas can efficiently couple to TEM transmission lines whose impedances are also independent of frequency.

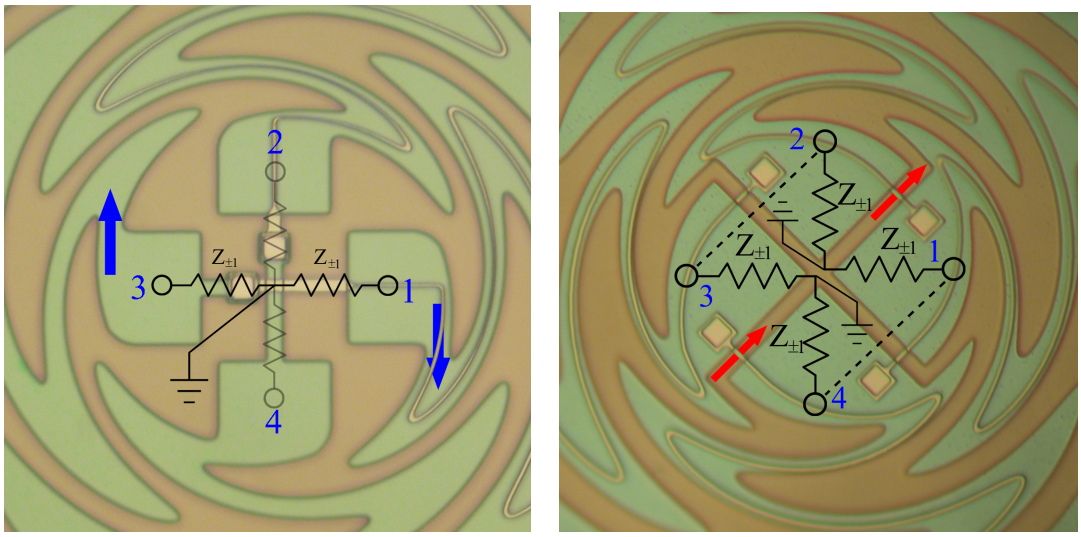

(a) H-V Excitation (b) $D_{\pm 45^o}$ Excitation

Figure 5.6. Photographs overlaid with effective circuits for the H-V and $D_{\pm 45^o}$ excitations. Green is ground plane, pink is microstrip, and rust-color is the slot carved between the antenna arms. There is a virtual ground in the center of each antenna and the blue and red arrows represent the excited electric and magnetic currents that travel outward to a $\lambda/2$ section where they radiate. When driven in the H excitation as shown in Figure (a), the resistors to 2 and 4 carry no current, so we grayed them out. When driven in the D_{+45^o} excitation as shown in Figure (b), port 2 is at the same potential as 3 and 1 is at the same as 4, as shown in the dashed lines. As a result, magnetic currents do not flow down the slots between these. Is it genuius, or the warped creation of a siphalitic mind?

Any linear combination of modes $M_{\pm 1}$ is also an eigenstate with that same impedance. In particular, excitations with just 180^o phase shifts between opposite arms (e.g. 1 and 3) and no power on the others (e.g 2 and 4) are an alternative sub-basis with the same eigenvalues $Z_{\pm}1$. These current patterns are the best choice for our applications since

they correspond to the linear polarizations we want to receive. The two linearly-polarized excitations V and H are:

$$(H, V) = M_{+1} \pm M_{-1} \tag{5.9}$$

where the minus sign refers to the V excitation. Note also that V has a 90^o phase shift from H in this definition.

These models for a free-space antenna break down when applied to our antennas that are fabricated on high-dielectric substrates. To convert our antenna into it's compliment, we must additionally exchange high permittivity materials with high permeability materials. Our sinuous antenna's compliment has to be on an extended hemisphere of high-μ material, so the antenna is not truly self-complimentary. In practice, it's input resistance will vary some with frequency and have a modest reactance. Despite this shortcoming of the model, we can invoke the popular approximation that the half-space is equivalent to a homogeneous space with an average permittivity:

$$\eta = \frac{\eta_o}{\sqrt{(\epsilon_o + \epsilon_{Si})/2}} \tag{5.10}$$

We have explored two methods to couple the integrated microstrip transmission lines to this antenna. The first (Figure 5.6(a)) places a gap-voltage between opposite arms (e.g.,1 and 3) by shoring the upper conductor of one of the two microstrips to the opposite arm's ground-plane. Since the effective circuit has two resistors of $Z_{\pm 1}$ in series between opposite arms, the total impedance, using Equations 5.7 and 5.10, is

$$Z_{in} = \frac{\eta_o}{\sqrt{1 + \epsilon_{lens}}} = 105\Omega \tag{5.11}$$

where the evaluation is for a silicon lens with $\epsilon = 11.8$. The two microstrips snake out on the back of the antenna arms and connect to the channelizer circuits in Chapters 7 and 8. Figure 5.7(a) shows ADS simulations of the input impedance $Z_{in} = Z_{11} - Z_{13}$ that agree with this model, but with the added reactance caused by the antenna nor being perfectly

self-complimentary. If the transmission lines have an impedance of 105 Ω, then the only 5% power is reflected at the interface on average. In practice, this is difficult to fabricate (See discussion in Chapter 6), but a 65 Ω line that is easier to fabricate results in a refleciton of only 8%.

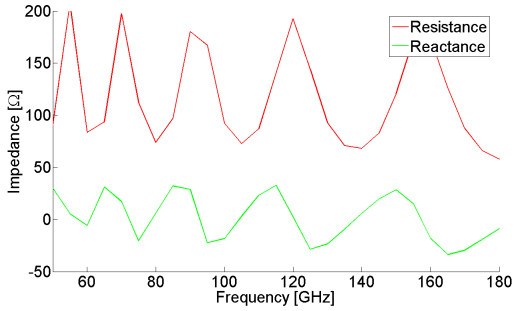

(a) Simulated Input Impedance on Silicon

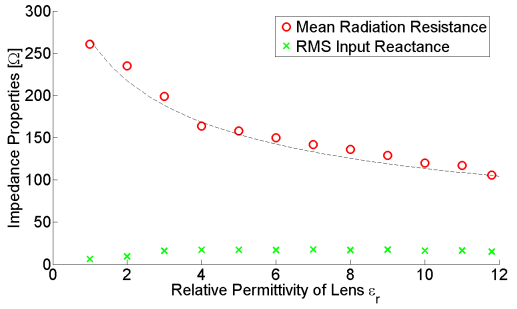

(b) Impedance characteristics in different lenses

Figure 5.7. Figure 5.7(a) shows ADS simulations of input impedance of a sinuous on silicon with the H-V feed. Results are similar for the $D_{\pm 45^o}$ excitation. Figure 5.7(b) shows how impedance properties change with the lens material. The right-most point is for silicon, the left is an antenna in free space. The dashed line is from Equation 5.11

Figure 5.7(b) shows the average input resistance $\bar{R}_{in}$ and RMS Reactance X_{in} as a function of lens permittivity. When $e_r = 1$ on both sides, the reactance nearly vanishes, but the impedance is a much higher 256 Ω.

Our second feeding scheme operates in a rotated basis that excites both of the linear and horizontal polarization modes simultaneously:

$$D_{\pm 45^o} = H \mp iV = (1 \pm i)M_{+1} + (1 \mp i)M_{-1} \tag{5.12}$$

where the notation $D_{\pm 45^o}$ reminds us that this polarization is on a diagonal between V and H. In this scheme, microstrips on the back of each arm short to adjacent arms through two resistors of $Z_{\pm 1}$, providing the same impedance as above. This is not surprising since the basis in Equation 5.12 is simply the dual of the feed in basis 5.9, and the antenna is presumed to be self-complimentary in this calculation. Opposite pairs of microstrips driven with a 180^o phase difference excite the two linear-polarizations in a manner that is very similar to the Polarbear detector antenna-feeds. The microstrips excite magnetic currents that travel outward in the slots between arms. Unfortunately, this feeding scheme also requires either a broadband balun or differentially feeding a lumped resistive load next to the TES to establish the required 180^o phase. The later option would greatly complicate the wiring by requiring several microstrip cross-overs and bias lines that cross the microstrips.

Finally, our collaborators at UCSD have devised a third feed. It is similar to the (H, V) feed, except that each polarization is excited by a pair of microstrips on opposite arms that meet in the middle without any vias to the ground plane. If the opposite arms have a 180^o phase shift, there will still be a virtual-ground in the center, but each arm will only see a termination of $Z_{\pm 1} = 53\Omega$, which is easier to match with Berkeley Microlab microstrips. Unfortunately, this still requires the same complicated wiring as the $D_{\pm 45}$ feed.

The team at UCSD is currently endeavoring to measure the impedance of these antennas in scaled models similar to those described in Section 5.7. However, the parasitic reactance associated with coupling the antennas to coaxial transmission lines have complicated their measurements and as of the writing if this thesis, they have not produced a conclusive result.

5.7 Sinuous Beam Patterns

As already described in Section 5.5, the antenna radiates and receives power on the $\lambda/2$ segments between switch-backs. So for a specific wavelength, a free space antenna's effective area should be proportional to λ^2. For a single-moded antenna, the throughput $A\Omega$ is also λ^2, so the antenna beam's solid angle of radiation Ω should vary little with frequency,

repeating every log-period. However, the contacting lens over the antenna establishes a specific scale (namely, the radius R) and breaks this self-similar nature of the antenna. As the wavelength drops, the beam will be narrow and if the lens is a synthesized ellipse, the beamwidth will drop as λ/R.

We felt it necessary to test the beam-patterns and cross-pol rejection of these designs in easy to fabricate cm-wavelength antennas before fabricating the millimeter devices. We worked closely with the UCSD team on these measurements and performed them in their anechoic chamber (*O'Brient et al.* [2008b]).

The Saturn Electronics Corporation made our antenna on a 0.635mm (0.025") thick substrate of Roger's 3010 with a relative permittivity of 10. The inner and outer radii of 0.24mm and 11.7mm provide upper and lower band edges of 12GHz and 5GHz. We fed the antenna by mounting low-barrier chip diodes (Metallic's MSS 30, 148-B10) across opposite arms in the center. In this way, the antenna is fed in the balanced version of the (H,V) excitations. We current biased the diodes with 240mA current provided by coaxial cables clad in Capcom EMI absorbing material. Finally, we rotated the antenna on a foam rotation stage in an anechoic chamber while horizontally facing a fixed standard gain horn (Dorado GH1-12N) 182cm (6'). The horn broadcasted a 1mW 1kHz and we measured the received power with a Stanford SR-830 lock-in amplifier.

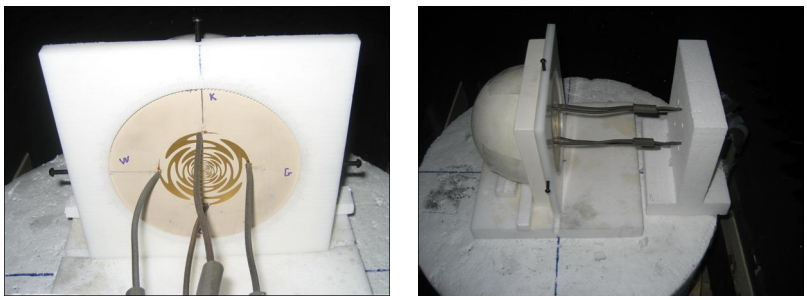

(a) Antenna Scale-Model

(b) Side-view of Eccostock extended hemispherical lens

Figure 5.8. Photographs of the 5-12GHz scale model antennas.

Figure 5.8 shows the antenna and lens on the rotating foam-platform in the UCSD anechoic chamber. The lens was made of Emmerson-Cuming's Eccostock HiK 12 material

whose index closely matches that of silicon. The hemisphere is 15.2 cm (6") in diameter and the extension is 3.8cm (1.5"), forming a lens that is beyond the elliptical point. A synthesized ellipse would have an extension 3.0cm (1.17") thick.

For our integration times of 5s, we observed a signal to noise ratio of roughly $S/N \sim 65$ that was constant for all sinuous antenna angles. This constant fractional noise is expected when the illuminating power is sufficiently strong that the noise is limited by the incident radiation and hence proportional to the incident power. The simulations predict a central-lobe beam-pattern that is roughly Gaussian, so $\log(P)$ should be linear with respect to θ^2. Taking the logarithms also removes the heteroscedasticity associated with the background limited noise, providing a standard deviation in log-space of $\delta P_i/_i P$ which is roughly constant.

Figure 5.9 shows the measured beam-patterns in the E and H planes co-plotted with ADS beam-simulations that were modified with the ray-tracing script developed in chapter 4. The cross-polarization is also low, at the 1-2% level, although our simulations routinely underestimate the cross-pol power.

The final figure of this group (Figure 5.9(e)) shows several co-plotted H-cuts at different frequencies to demonstrate that the beams narrow with increasing frequency as advertised. We fit gaussian profiles to the patterns above the 10dB power level and found a strong fit with reduced χ^2 between 0.6 and 1.4. Figure 5.10 plots the fit gaussian beam waists vs frequency for both E and H plane, and the solid lines are simulation predictions. Clearly, the simulations and data follow similar trends and have similar values, but the tight error bars on the data preclude a statistically significant agreement.

There are other more subtle disagreements between simulations and measurements. Most notably, the measured beams show subtle asymmetries. Since our direct involvement, the team at UCSD has demonstrated that the asymmetries are caused by inhomogeneities in the eccostock itself and that they vanish when the eccostock lens is replaces with a silicon one. The simulations predict stronger side-lobes than the measured beams, but our collaboration has found that these are strongly suppressed both in simulations and

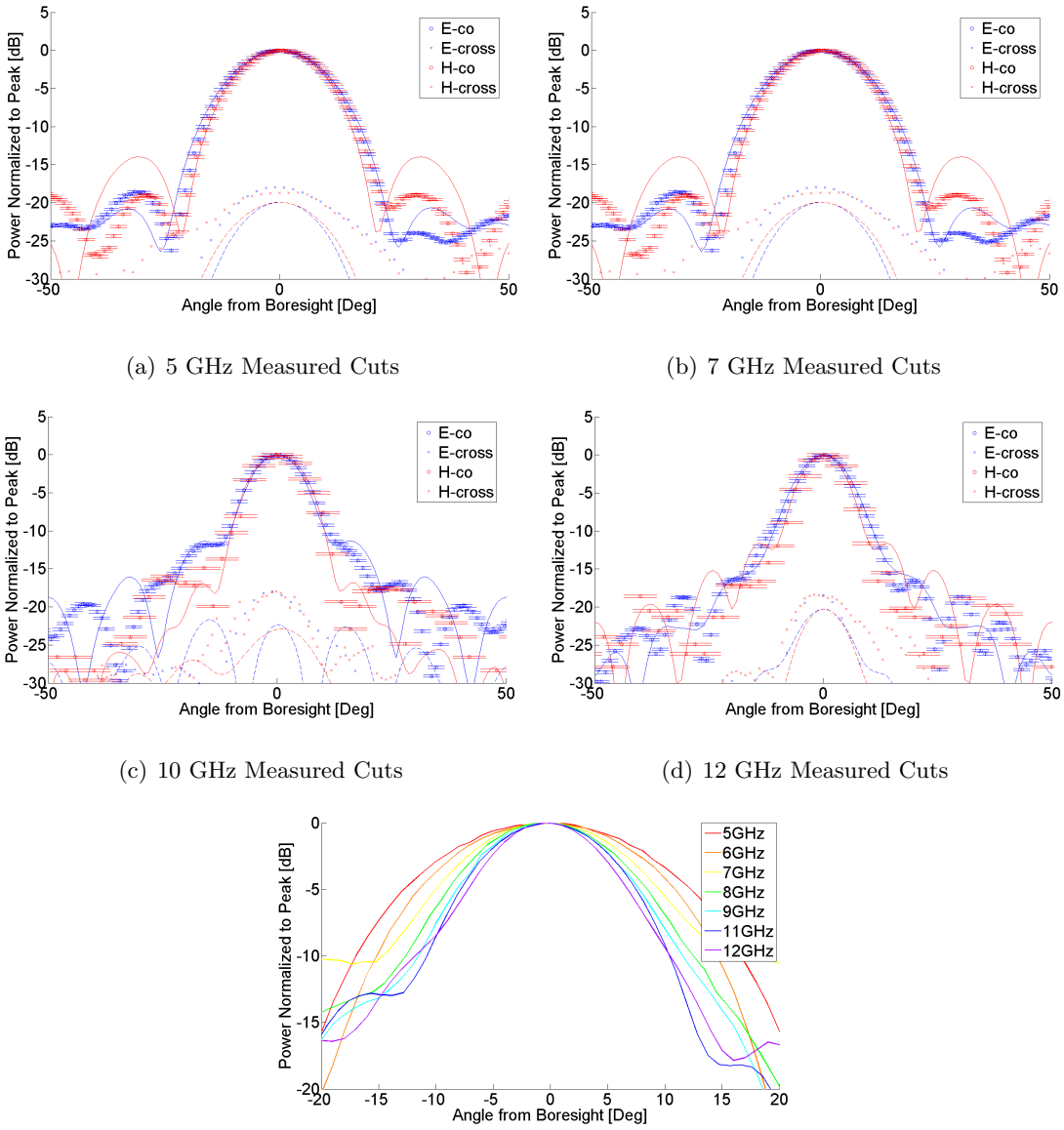

(a) 5 GHz Measured Cuts

(b) 7 GHz Measured Cuts

(c) 10 GHz Measured Cuts

(d) 12 GHz Measured Cuts

(e) Several channels of H cuts

Figure 5.9. Measured beam-patterns on scale mode devices. Blue is E-plane and red is H-plane. The circular markers are co-polarized while the x-markers are cross-polarized. The solid and dashed curves are simulations for co- and cross-polarization. The last picture shows several H-plane cuts co-plotted.

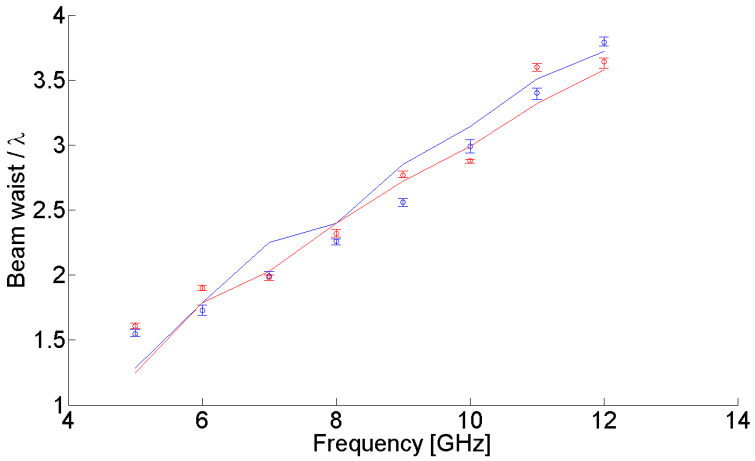

Figure 5.10. Gaussian Beam-waist vs Frequency. Solid lines are simulation

measurements by adding an anti-reflection (AR) coating to the lens. The UCSD team used quarter wavelength rexolite coatings on their silicon lens to suppress the sidelobes and also to suppress the cross-polarized power to under the -20dB level.

The silicon lens that UCSD is currently using is a synthesized ellipse of silicon with 5.08cm (2") diameter and they are testing it with a smaller antenna. Additionally, they mounted the feed-horn on it's own rotational stage to control the polarization tilt angle of the incident wave and to demonstrate the wobble shown in Figure 5.11. This amplitude is appears to be consistent with our simulations, although the UCSD team has not yet done a full statistical comparison. The tilt does not perfectly repeat after a log-period, as seen in both measurements and simulation *Edwards* [2008]. We do not yet understand the origin of this effect, but it is sufficiently subtle that we do not anticipate it compromising the polarization properties in our prototype detectors.

5.8 Conclusions

This chapter introduced the sinuous antenna as a log-periodic with desirable polarization properties on a contacting dielectric lens. We also derived the approximate input impedance for a self-complimentary antenna (δ=22.5^o). Finally we tested the design in 5-12GHz "scale-

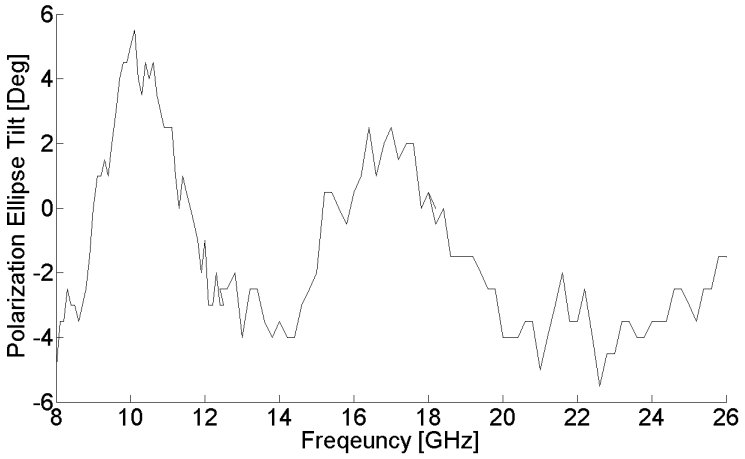

Figure 5.11. Polarization tilt τ vs frequency. The tilt oscillates $\pm 4^o$ every log-periodic scaling of frequency 1.3^2. Thanks to Jen Edwards for providing this figure (*Edwards* [2008]).

model" devices to verify that the design had beam patterns consistent with our simulations. The initial results show some deviations, but were none-the-less encouraging. Since then, the UCSD team has suppressed many of the high side-lobe and cross-pol levels in their measurements by changing lens materials and adding an AR-coating, providing data that agrees much more closely with the models. Meanwhile, the Berkeley side of the collaboration proceeded to fabrication and testing of the millimeter devices described in chapters 6-8.